How to cite: *Angew. Chem. Int. Ed.* **2022,** *61,* e202203063
International Edition: doi.org/10.1002/anie.202203063
German Edition: doi.org/10.1002/ange.202203063

CO_2 Methanation

Highly Selective Photocatalytic CO_2 Methanation with Water Vapor on Single-Atom Platinum-Decorated Defective Carbon Nitride

Xianjin Shi, Yu Huang, Yanan Bo, Delong Duan, Zhenyu Wang, Junji Cao,* Gangqiang Zhu, Wingkei Ho, Liqin Wang, Tingting Huang, and Yujie Xiong**

Abstract: Solar-driven CO_2 methanation with water is an important route to simultaneously address carbon neutrality and produce fuels. It is challenging to achieve high selectivity in CO_2 methanation due to competing reactions. Nonetheless, aspects of the catalyst design can be controlled with meaningful effects on the catalytic outcomes. We report highly selective CO_2 methanation with water vapor using a photocatalyst that integrates polymeric carbon nitride (CN) with single Pt atoms. As revealed by experimental characterization and theoretical simulations, the widely explored Pt–CN catalyst is adapted for selective CO_2 methanation with our rationally designed synthetic method. The synthesis creates defects in CN along with formation of hydroxyl groups proximal to the coordinated Pt atoms. The photocatalyst exhibits high activity and carbon selectivity (99 %) for CH_4 production in photocatalytic CO_2 reduction with pure water. This work provides atomic scale insight into the design of photocatalysts for selective CO_2 methanation.

Introduction

The solar-driven CO_2 photoreduction into value-added products is a fascinating way of simultaneously addressing greenhouse gas emission challenge and producing profitable fuel.[1] To this end, numerous photocatalysts have been developed for CO_2 photoreduction, including metal-containing materials (e.g., metal oxides,[2] metal sulfides,[3] metal–organic frameworks[4]) and metal-free materials (e.g., graphene oxide,[5] carbon nitride[6]). Despite the relatively high selectivity for CO production, highly selective CO_2 methanation with water (i.e., the conversion of CO_2 and H_2O to CH_4 without the assistance of sacrificial agent) is still a challenge to photocatalysis.[7] It is well known that the photocatalytic conversion of CO_2 and H_2O to CH_4 is a typical multi-electron reduction process.[8] Such a process sets up high criteria for photocatalyst design: *i*) active sites should be capable of accumulating abundant photogenerated electrons to facilitate the conversion process; *ii*) the hydrogen atoms generated from H_2O reduction should be preferentially delivered to the active sites, where CO_2 is adsorbed and activated, for forming C–H bonds instead of undergoing H_2 evolution. As such, the design of active sites together with semiconductor selection is the key to achieving highly selective CO_2 methanation via photocatalysis.

In terms of semiconductor selection, polymeric carbon nitride (CN) is an attractive candidate for photocatalytic CO_2 reduction reactions owing to its visible-light response, earth abundance and high stability.[6,9] However, the major limitation for CO_2 photoreduction originates from the C–N forming π-conjugated planes along which charge migration is impeded. As a result, the rapid recombination of photogenerated carriers kinetically limits the efficiency of CO_2 photoreduction over CN.[10] To overcome the limitation, tremendous efforts, such as element doping,[11] heterojunction constructing,[12] and nanostructure tailoring,[6] have been

[*] X. Shi, Prof. Y. Huang, Z. Wang, L. Wang, T. Huang
Key Laboratory of Aerosol Chemistry and Physics, State Key Laboratory of Loess and Quaternary Geology (SKLLQG), Institute of Earth Environment, Chinese Academy of Sciences
Xi'an, 710061 (P. R. China)
E-mail: huangyu@ieecas.cn

X. Shi, Prof. Y. Huang, Z. Wang, L. Wang, T. Huang
Center of Excellence in Quaternary Science and Global Change, Chinese Academy of Sciences
Xi'an, 710061 (P. R. China)

X. Shi
University of Chinese Academy of Sciences
Beijing, 100049 (P. R. China)

Y. Bo, D. Duan, Prof. Y. Xiong
School of Chemistry and Materials Science, University of Science and Technology of China
Hefei 230026 (P. R. China)
E-mail: yjxiong@ustc.edu.cn

Prof. J. Cao
Institute of Atmospheric Physics, Chinese Academy of Sciences
Beijing, 100190 (P. R. China)
E-mail: jjcao@mail.iap.ac.cn

Prof. G. Zhu
School of Physics and Information Technology, Shaanxi Normal University
Xi'an, 710062 (P. R. China)

Prof. W. Ho
Department of Science and Environmental Studies, The Education University of Hong Kong
Hong Kong (P. R. China)

devoted to maneuvering charge dynamics. Nevertheless, these strategies are incapable of localizing photogenerated electrons over the active sites where CO_2 is adsorbed and activated. For this reason, introduction of metal atoms to the π-conjugated planes has been widely explored.[8b,13] Taking advantage of C–N units, the metal atoms can be facilely coordinated with the π-conjugated planes, which not only serve as active sites to enhance catalytic performance[14] but also facilitate charge separation and transport.[15] Among the metals, Pt appears to be the best one for localizing photogenerated electrons, and can be rationally engineered into single-atom sites in integration with CN.[16] The single Pt atoms have been proven to serve as active sites for photocatalytic reactions along with C=N bond reconstruction,[17] paving the way to exploring their potential in photocatalytic CO_2 methanation. Although such a catalyst combination of Pt–CN meets the requirement for electron localization, the application of photocatalytic CO_2 methanation still suffers from the competition reaction H_2 evolution that very easily takes place at Pt sites when H_2O is employed as hydrogen source. Certainly, the H_2 evolution can be suppressed to some extent by turning H_2O supply to vapor phase; however, the evolution of H atoms into H_2 still undoubtedly exceeds the formation of C–H bonds if the H atoms are formed at the Pt sites. This situation raises a fundamental question whether such a widely explored Pt–CN catalyst combination can be reinvented to make the electron-rich Pt sites preferentially work for CO_2 activation while the formation and supply of H atoms take place at other sites of π-conjugated planes.

In this work, we rationally developed a synthetic method for controlling the local environment of single-atom Pt to reinvent the Pt–CN catalyst combination. In the reinvented configuration, isolated Pt atoms were coordinated with CN to localize photogenerated electrons as evidenced by light-assisted Kelvin probe force microscopy (KPFM) and time-resolved surface photovoltage spectra (TR-SPV). More importantly, our synthetic method created defects and formed hydroxyl (–OH) groups in the CN in neighbor with the coordinated Pt atoms. While the Pt sites were designated for CO_2 adsorption and activation, the neighbored –OH groups made the formation of H atoms preferentially occur on CN, overcoming the existing limitation of Pt–CN in photocatalytic CO_2 reduction. In situ Fourier-transform infrared (FTIR) spectroscopy and density functional theory (DFT) calculations indicated that the localized electrons at Pt sites selectively activated the adsorbed CO_2, which in turn formed C–H bonds with the H atoms supplied from the CN. In the meantime, the binding of *CO reaction intermediate to Pt sites was substantially strengthened, avoiding the formation of CO byproduct. Such a catalyst design enabled the high carbon-based selectivity (99 %) for CH_4 production in a pure water system. This work provides a new insight for the design of photocatalysts at the atomic scale to tune reaction pathways in multi-electron CO_2 photoreduction process.

Results and Discussion

The photocatalyst (noted as Pt@Def-CN) was prepared by immobilizing the isolated Pt atoms on the defective CN, as schematically illustrated in Figure 1a. First, a primitive CN (noted as P-CN) was fabricated by thermal condensation melamine. As shown in Figure 1b, the two typical X-ray diffraction (XRD) peaks of P-CN centered at 13.2° and 27.4° were attributed to the long-range ordered tri-s-triazine units and the interlayer stacking of conjugated aromatic groups, respectively.[18] Second, a defective CN (noted as Def-CN) was synthesized through hydrothermal treatment of P-CN. The XRD peak for Def-CN at 13.2° disappeared and a new XRD peak arose at 10.7° with the increase of the hydrothermal treatment time (Figure 1b and Figure S1). This reveals that the partial dissociation of the intralayer tri-s-triazine units during the hydrothermal process results in the formation of –OH groups. This feature was confirmed by the appearance of a peak at 1084 cm^{-1} and a broad peak at around 3000–3600 cm^{-1} for the vibration signals of C–O and O–H in FTIR spectroscopy (Figure 1c).[19] Third, the single Pt cationic groups were introduced precisely to the defective edges of the Def-CN, in which the coordination as well as the electrostatic force between the Pt cationic groups and the negatively charged oxygen-containing functional groups played the role, to form an intermediate. Finally, the intermediate was calcinated at low temperature to tightly bind the Pt atom with the CN material. The XRD peaks (Figure 1b) and FTIR spectra (Figure 1c) of Pt@Def-CN are the same as those of Def-CN while no other peaks appeared, indicating that the presence of Pt atoms did not affect the structure of the CN materials.

To resolve the distribution of Pt on the Pt@Def-CN catalyst, aberration-corrected high-angle annular dark-field scanning transmission electron microscopy (AC-HAADF-STEM) was employed to characterize Pt@Def-CN. Figure 1d and e clearly showed that a large number of bright spots corresponding to heavy Pt atoms were atomically dispersed on the defective support while no obvious agglomerated Pt clusters or particles were observed, suggesting that Pt species were mainly distributed as isolated atoms on the Def-CN support. Furthermore, energy-dispersive spectroscopy (EDS) mapping revealed the uniform dispersion of Pt atoms on the support materials (Figure 1f). The Pt loading content of Pt@Def-CN was as high as 1.08 wt % measured by inductively coupled plasma-mass spectrometry (ICP-MS). Note that at such a high Pt loading, no Pt clusters or particles were found by transmission electron microscopy (TEM) (Figure S2). Taken together, the characterizations indicated that Pt was successfully loaded on the surface of the catalyst in the form of single atoms.

To determine the local coordination structure of single Pt atoms, the catalyst was further examined by X-ray absorption fine structure spectroscopy (XAFS). Figure 2a showed the normalized Pt L_3-edge X-ray absorption near-edge structure (XANES) spectra of the Pt@Def-CN catalysts with reference to the standard Pt foil and PtO_2. The white-line intensity of the Pt@Def-CN was higher than that of Pt foil and lower than that of PtO_2, suggesting that single

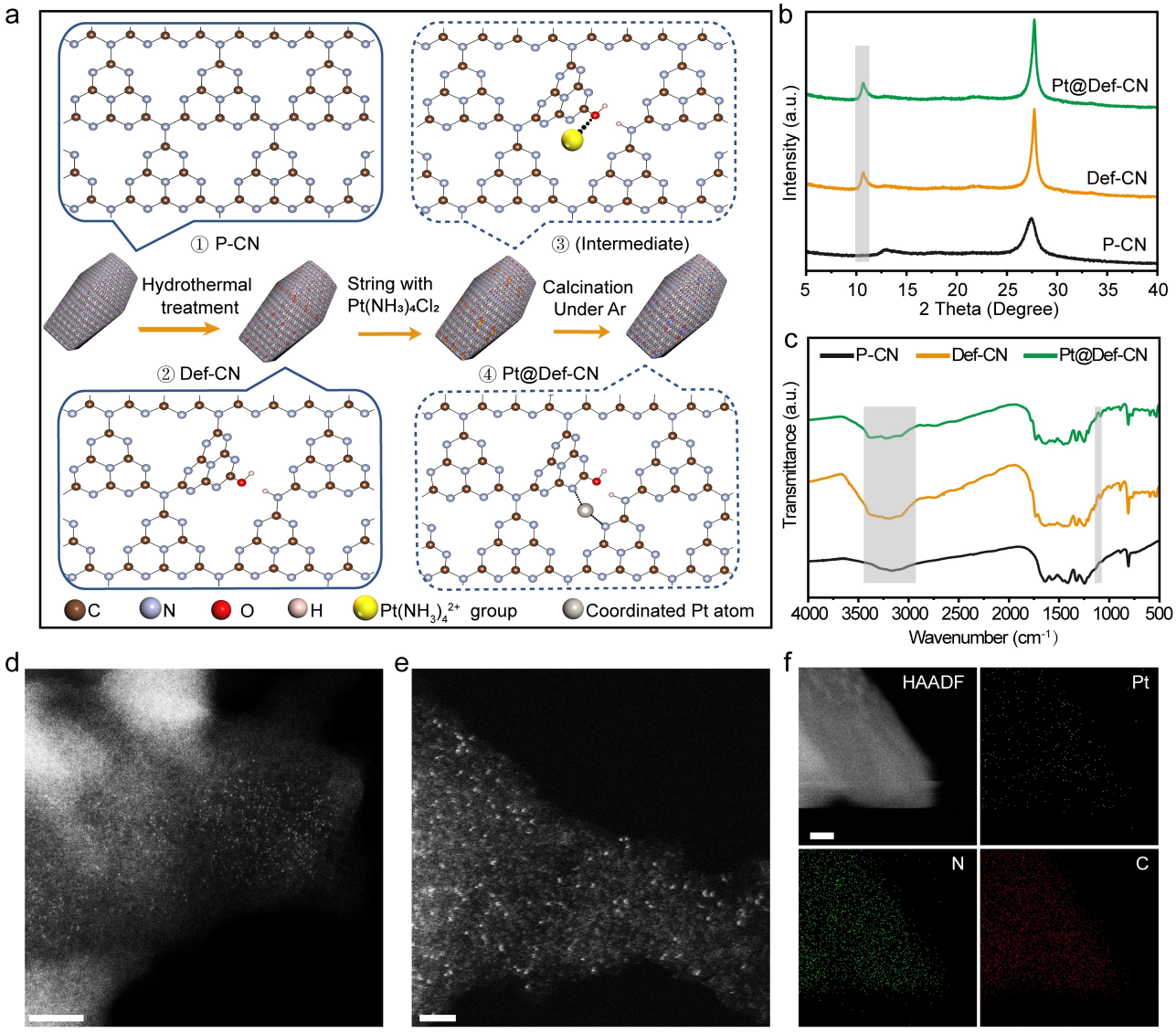

Figure 1. a) Schematic illustration for the synthesis of the Pt@Def-CN. b) XRD patterns and c) FTIR spectra of P-CN, Def-CN and Pt@Def-CN. d, e) AC-HAADF-STEM image of Pt@Def-CN. f) EDS mapping of Pt@Def-CN. Scale bar: d) 10 nm; e) 2 nm; f) 5 nm.

Pt atoms carried a partial positive charge ($Pt^{\delta+}$, $0<\delta<4$). This finding was consistent with Pt 4f X-ray photoelectron spectroscopy (XPS) which showed peaks shift toward higher binding energies as compared with metal Pt (Figure S3). The results illustrated the strong interactions between the single Pt atoms and the support material, which would be beneficial to electron transport.[20]

Fourier-transformed extended X-ray absorption fine structure (FT EXAFS) in R space was performed to determine the local structures of the single Pt atoms (Figure 2b). With reference to standard Pt foil, the Pt L_3-edge k^3-weighted FT EXAFS of Pt@Def-CN sample displayed one main peak at 1.57 Å and no peak corresponding to the Pt–Pt bond (2.57 Å). This excluded the formation of metallic crystalline Pt clusters or particles and confirmed the sole existence of isolated Pt atoms, consistent with the AC-HAADF-STEM results. To reinforce these results, wavelet-transform (WT) contour plots of Pt@Def-CN, Pt foil and PtO_2 were analyzed (Figure 2c). Compared with those of the Pt foil and PtO_2, WT plots of Pt@Def-CN showed only one intensity maximum at 3.9 $Å^{-1}$, which can be assigned to Pt–N/C/O coordination. This suggested that the Pt atoms on Pt@Def-CN existed as isolated Pt atoms without the presence of metallic Pt crystalline structures.

Quantitative least-squares EXAFS was also used to analyze the coordination of single Pt atoms in Pt@Def-CN (Figure 2b, Figure S4, and Table S1). The analysis revealed that the coordination number was 2.0 ± 0.23 with the distance of 1.94 ± 0.03 Å, significantly lower than the coordination number of 6 at the center of the six-fold cavity and the coordination number of 5 at the top of the five-membered rings.[16] This illustrated that the Pt atoms were dispersed on a defective structure of the CN network. Given that Pt–O, Pt–N and Pt–C coordination can be hardly

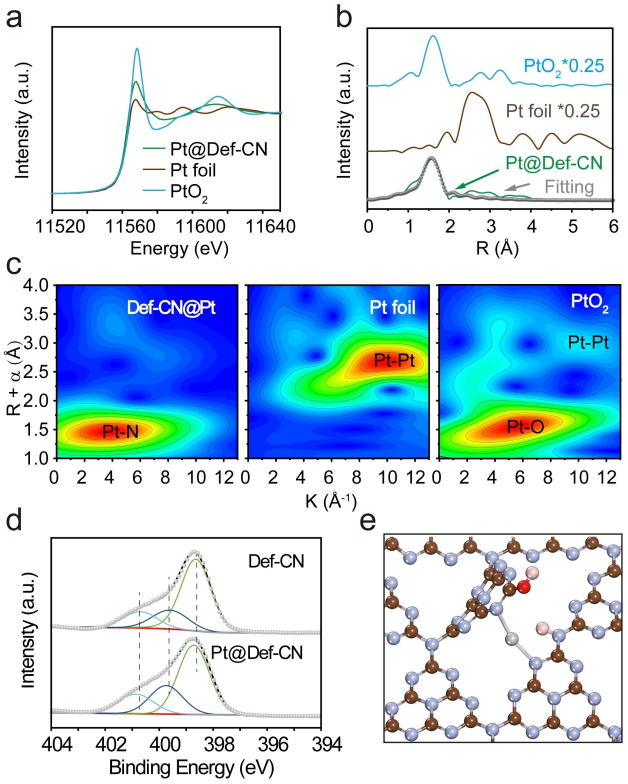

Figure 2. a) Normalized Pt L_3-edge XANES spectra. b) k^3-weighted Fourier-transform Pt L_3-edge EXAFS spectra of Pt@Def-CN, Pt foil and PtO_2, and fitting curve of Pt@Def-CN in R space. The note *0.25 means that the curve value shown here is equal to the original value multiplied by 0.25. c) WT of Pt@Def-CN, Pt foil and PtO_2. d) N 1s XPS spectra of Pt@Def-CN and Def-CN. e) Local atomic structure around Pt. Color code: carbon is brown, oxygen is red, hydrogen is pink, nitrogen is gray, and Pt is dark gray.

distinguished, XPS characterization was also used to analyze the coordination location of single Pt atoms on the support surface. The N 1s spectra in Def-CN at 398.6, 399.6 and 400.7 eV, which were assigned to sp^2-bonded nitrogen C–N–C, sp^3 tertiary nitrogen N–C_3 and C–NH_x, respectively (Figure 2d).[21] After the introduction of single Pt atoms, the XPS peaks of C–N–C, HN–C_3 and C–NH_x shifted toward higher binding energies, indicating that the electron density of N atoms was reduced by the coordination with single Pt atoms.[16] In sharp contrast, the C 1s and O 1s XPS of Pt@Def-CN did not display similar phenomena to the N 1s XPS (Figure S3). This revealed that the unsaturated Pt atoms were dispersed on the defect locations of the CN material by coordination with two N atoms, as illustrated in Figure 2e.

The photoreduction of CO_2 performance for the as-obtained photocatalysts was evaluated in a batch reactor under simulated solar illumination conditions in a pure-water system. Control experiments in dark or without the photocatalyst did not show the evolution of CO or CH_4, suggesting that photocatalysts and light irradiation were necessary for the photoreduction of CO_2. The measurements showed that Pt@Def-CN offered a CH_4 evolution of 6.3 $\mu mol\,g^{-1}\,h^{-1}$, reflecting the high efficiency of our catalyst in the photoreduction of CO_2 to CH_4 in a pure H_2O system (Table S2). The performance of CO_2 photoreduction into CH_4 for Pt@Def-CN was enhanced by 20 and 3 times compared with those of P-CN (0.3 $\mu mol\,g^{-1}\,h^{-1}$) and Def-CN (2.1 $\mu mol\,g^{-1}\,h^{-1}$), respectively (Figure 3a). This demonstrated that the Pt sites at the defect locations greatly improved the CO_2 photoreduction performance. In the meantime, only a small fraction of photogenerated electrons (about 3%) are used for side product H_2 production, indicating that the addition of Pt sites in our catalyst did not significantly cause the promotion of H_2 evolution. For

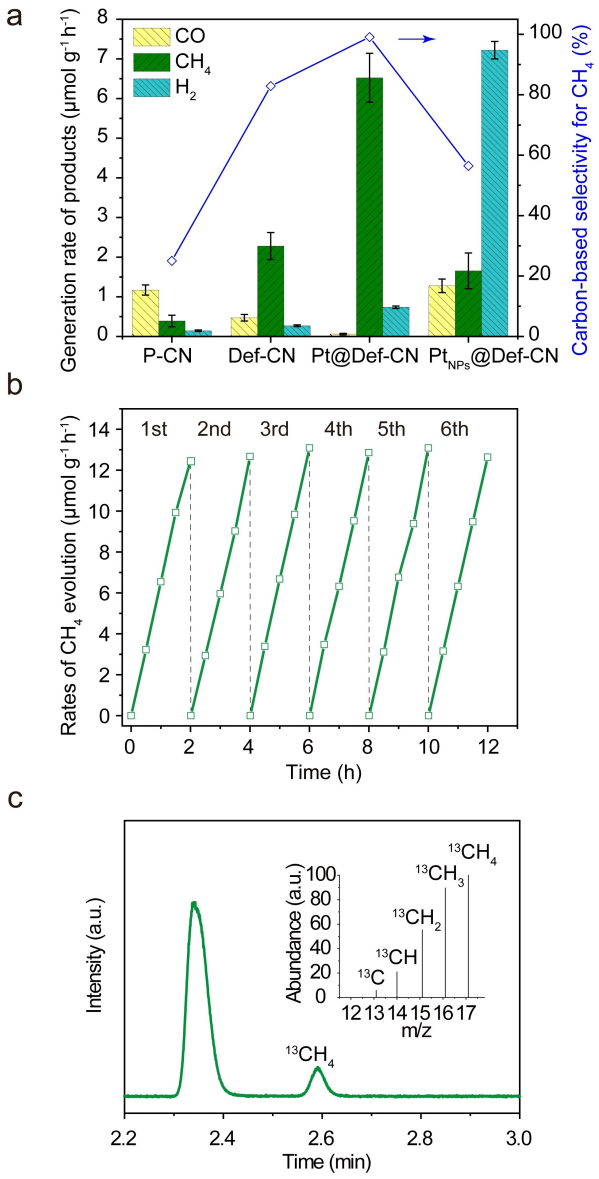

Figure 3. a) Conversion and carbon-based selectivity of photocatalytic CO_2 reduction with H_2O into CO, CH_4 and H_2 over P-CN, Def-CN, Pt@Def-CN, and Pt_{NPS}@Def-CN. Each value is the average of three tests, and the standard deviation of these measurements is indicated by error bars. b) Stability of Pt@Def-CN during six photocatalytic cycles. c) GC-MS analysis of $^{13}CH_4$ products for photocatalytic $^{13}CO_2$ reduction over Pt@Def-CN.

comparison, traditional metallic Pt nanoparticles (NPs) were integrated with Def-CN to form a reference sample (namely, Pt_{NPs}@Def-CN) (Figure S5). As shown in Figure 3a, the main product of Pt_{NPs}@Def-CN is H_2 (7.2 μmol g^{-1} h^{-1}) rather than CH_4 (1.7 μmol g^{-1} h^{-1}) under the same conditions.

Carbon selectivity is another key factor to the CO_2 photoreduction performance. As a reference, P-CN showed a low CH_4 selectivity (25 %) while the major product was CO. After creating defects, the carbon selectivity for CH_4 production was increased to 78 % by Def-CN. Impressively, our Pt@Def-CN showed the dramatically enhanced carbon selectivity for CH_4 production up to 99 %, demonstrating that the CO production was almost prevented. We also examined the other half reaction—O_2 production, which turned out to undergo at a rate of 12.4 μmol g^{-1} h^{-1} (Figure S6). It is noteworthy that the evolution rate ratio of CH_4 to O_2 approached to the stoichiometric ratio of 0.5, manifesting that the reaction of CO_2 with H_2O took place indeed.[22] Moreover, the CH_4 evolution can be largely maintained after six cycles of reactions (Figure 3b), as the structure and morphology of catalyst remained unchanged (Figures S7 and S8), illustrating the excellent durability of our catalyst. Furthermore, the isotope labelling experiment was used to verify the origin of CH_4. The fragment peaks of $^{13}CH_4$ can be detected at m/z = 17, 16, 15, 14 and 13 when $^{13}CO_2$ was used as the reactant (Figure 3c). In sharp contrast, the product of $^{12}CH_4$ displayed the fragment peaks at m/z = 16, 15, 14, 13 and 12 in the mass spectra with the $^{12}CO_2$ gas as the reactant (Figure S9). This confirmed that CH_4 did originate from the photocatalytic reduction of CO_2. Taken together, the measurements demonstrated that our Pt@Def-CN catalysts offered high activity in photocatalytic CO_2 reduction as well as high carbon selectivity for CH_4 production.

To clarify the mechanism of the improved photocatalytic performance, three elementary processes including light absorption, charge separation and surface reactions should be taken into consideration.[23] After loading Pt, Pt@Def-CN did not show a significant difference in the UV/Vis diffuse reflectance spectra (Figure S10), suggesting that the great improvement in the photocatalytic performance by Pt@Def-CN was not ascribed to the change of light absorption. We thus looked into the other two factors—charge separation and surface reactions.

To disclose the location of the photo-induced electrons at the nanometer scale, light-assisted KPFM was employed to characterize the system.[24] While the KPFM image of Pt@Def-CN in the dark state showed the same features as the atomic force microscopy (AFM) image (Figures 4a and b), the contact potential difference (CPD) of the Pt@Def-CN was about 50 mV (CPD_{dark}). After light irradiation was turned on, the CPD of the Pt@Def-CN was increased to 150 mV (CPD_{light}) (Figure 4c) although no change was observed for image features. According to previous reports,

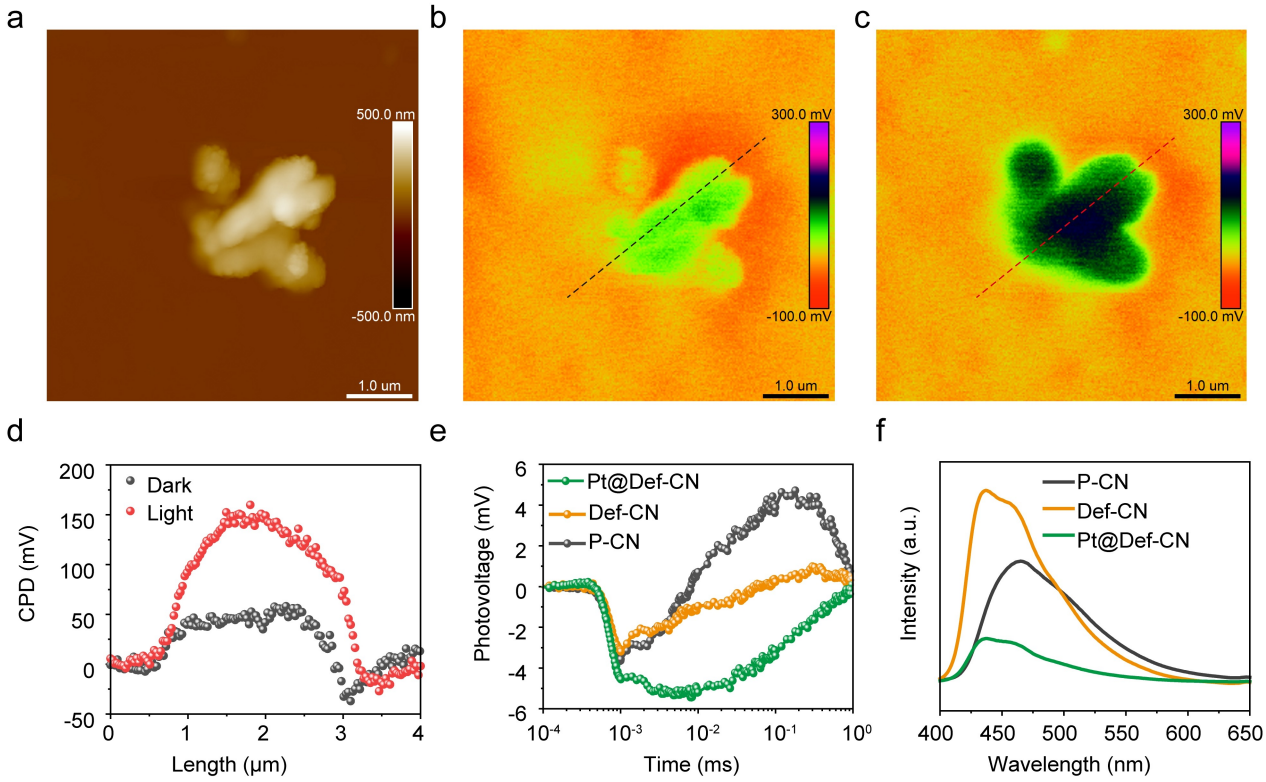

Figure 4. a) AFM topography image of Pt@Def-CN. KPFM image of Pt@Def-CN b) in dark and c) under light illumination. d) CPD profiles of dark state and light state across the black line in (b) and red line in (c). e) TS-SPV response for P-CN, Def-CN, and Pt@Def-CN. f) Steady-state PL spectra of P-CN, Def-CN, and Pt@Def-CN.

surface electron concentration should be positively correlated with the change of surface potential.[25] The surface potential across the Pt@Def-CN sample under light irradiation was nearly 100 mV higher than that in dark state (Figure 4d). In sharp contrast, the change of CPD for P-CN and Def-CN was substantially smaller than that of Pt@Def-CN after turning on light (Figures S11 and S12). This indicated that more photogenerated electrons were localized on the surface of the Pt@Def-CN catalyst during the illumination process.

TR-SPV measurements were further employed to track the dynamical features of the photogenerated charge carriers (Figure 4e).[26] In the initial stage of photovoltage generation (at $\approx 10^{-6}$ s), the obtained samples all showed a negative photovoltage response as the separation of photogenerated charges was dominated by the trapping of photogenerated electrons on surface. Subsequently, a positive photovoltage response occurred (at $\approx 10^{-4}$ s) for P-CN. Owing to the existing defects in the in-plane structure, no positive photovoltage response was observed for Def-CN as anticipated. In stark contrast, Pt@Def-CN maintained a larger time scale (at $\approx 10^{-5}$ s) and a high surface negative voltage, suggesting that the isolated Pt atoms at the defective edge served as trap states to localize more photogenerated electrons on the catalyst surface.

Such an electron trapping effect by single Pt atoms effectively reduced the recombination of photogenerated charges, which in turn significantly suppressed the recombination-associated emission as demonstrated by steady-state photoluminescence (PL) spectroscopy (Figure 4f). Def-CN displayed a stronger intrinsic emission peak than P-CN due to the existing abundant charge recombination centers.[27] However, after the introduction of single Pt atoms at the defect edges, Pt@Def-CN exhibited the significantly damped emission, suggesting the reduced charge recombination rate. It is worth mentioning that the PL intensity of Pt@Def-CN is even dramatically weaker than P-CN, demonstrating that the single Pt atoms at defect edge served as electron traps indeed. Moreover, single Pt atoms can increase the utilization efficiency of photogenerated charge carriers toward redox reactions, as confirmed by photocurrent responses and electrochemical impedance spectroscopy (EIS) (Figure S13). This fact should be beneficial for the 8-electron CO_2 reduction process kinetically.

To better demonstrate the role of single Pt atoms, a series of catalysts with different loading amounts of single atoms Pt were synthesized (Figure S14). The number of electrons participating in the reaction was boosted by increasing the amount of single Pt atoms (Figure S15), suggesting that single Pt atoms can effectively improve the utilization rate of photogenerated electrons. Notably, the single Pt atoms-based catalysts exhibited the high selectivity for CO_2 methanation versus H_2 evolution, which urged us to reveal the key catalyst parameter to the product selectivity. Accordingly, we identified the parameter based on the performance of Pt_{NPS}@Def-CN, which turned out to mainly produce H_2 rather than CH_4 in the reaction. This finding is consistent with the common feature reported in literature that Pt is one of the best cocatalysts for efficiently collecting photogenerated electrons and promoting H_2 evolution.[28] Such a feature of Pt nanoparticles inevitably reduced the selectivity of CO_2 methanation. Taken together, the results above proved that the Pt loading in the form of single atoms has promoted the utilization of photogenerated electrons specifically toward CO_2 methanation.

Upon identifying the electron localization at single Pt atoms, we are now in a position to decode the mechanism for selective photocatalytic CO_2 methanation. As CO_2 adsorption is a prerequisite for CO_2 photoreduction, we first analyzed the CO_2 adsorption behavior. Our measurement showed that the CO_2 adsorption capacity of Def-CN and Pt@Def-CN was nearly ten times higher than that of P-CN (Figure 5a), suggesting that the defective structure with –OH groups facilitated the adsorption of CO_2 on the catalyst surface. Note that the three samples possess similar morphology and hydrophilicity (Figures S16 and S17) but different specific surface area and pore structure (Table S3 and Figure S18). The specific surface area increased from 9.6 $m^2 g^{-1}$ of P-CN to 19.6 $m^2 g^{-1}$ of Def-CN and 19.5 $m^2 g^{-1}$ of Pt@Def-CN. Furthermore, the activation of CO_2 at the active sites was demonstrated by in situ FTIR spectroscopy.[3,29] As shown in Figure 5b, after exposing Pt@Def-CN to CO_2/H_2O vapors and light, the peaks at 1236, 1319, 1597 and 1633 cm^{-1} that should attributed to the formation of HCO_3^- arose. Such a HCO_3^- intermediate was derived from the CO_2 captured by the –OH group.[30] A *COOH absorption peak at 1766 cm^{-1} appeared and then reached equilibrium with increasing irradiation time owing to equilibrium between *COOH consumption and CO_2 adsorption.[31] Moreover, the signals of reaction intermediates such as *CHO (1396 and 1454 cm^{-1}), *CH_2O (1419 cm^{-1}) and *CH_2 (1374 cm^{-1}) were detected.[30a,c,32] As reported in literature, the direct breakage of C=O bond in the *CH_2O groups is kinetically slow, suggesting the existence of an intermediate (*CH_2OH) from *CH_2O to

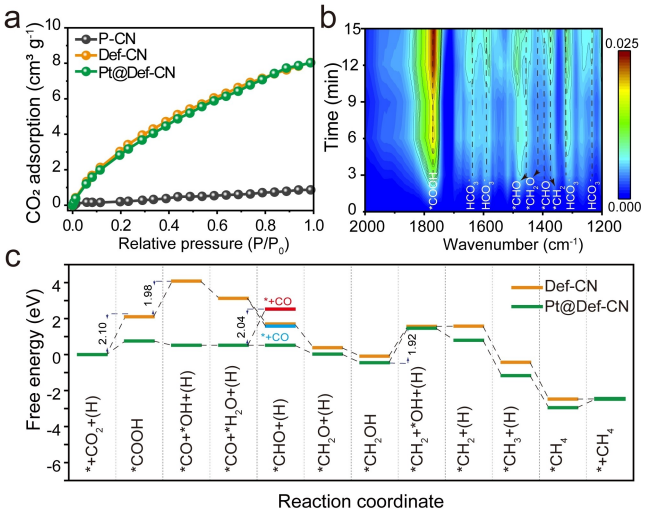

Figure 5. a) CO_2 adsorption isotherm of P-CN, Def-CN and Pt@Def-CN. b) In situ FTIR spectra for the CO_2 reduction process over Pt@Def-CN. c) Calculated free-energy diagram for CO_2 reduction to CH_4 on the Pt@Def-CN catalyst and Def-CN catalyst.

$^*CH_2$.[30a] Once $^*CH_2$ was formed, it would easily evolve into $^*CH_4$ by subsequent hydrogenation.[30a,33] Based on the information gleaned above, we can summarize the reaction pathway for photoreduction of CO_2 into CH_4 as follows:

$$CO_2 \rightarrow {}^*CO_2 \rightarrow {}^*COOH \rightarrow {}^*CO \rightarrow {}^*CHO \rightarrow {}^*CH_2O \rightarrow {}^*CH_2OH \rightarrow {}^*CH_2 \rightarrow {}^*CH_3 \rightarrow {}^*CH_4 \rightarrow CH_4$$

To compare the reaction processes on Def-CN and Pt@Def-CN, the thermodynamics of reactions from CO_2 on two surfaces were further investigated using DFT calculations (Figures 5c, S19 and S20). For CO_2 reduction to CH_4 on the Def-CN, the formation of *COOH and *CO were highly endergonic processes with free enthalpy of 2.10 eV and 1.98 eV, respectively. However, after incorporating Pt on Def-CN, the free enthalpies of *COOH (0.75 eV) and *CO (−0.23 eV) were lowered, thereby turning the thermodynamic limiting step to the formation of $^*CH_2$ (1.92 eV). Furthermore, we found that *CO can easily desorb from the Def-CN surface, while desorption of *CO from the Pt@Def-CN was a highly endergonic process (2.04 eV). This well explained why the introduction of Pt single atoms turned the product selectivity from CO to CH_4.

Another puzzle for the Pt@Def-CN is the reason why the use of Pt sites did not boost H_2 evolution. It has been reported that the reduction in the size of Pt nanoparticles adversely affects the selectivity of CH_4 during CO_2 photoreduction.[34] To unravel the puzzle, we simulated the binding of H atoms to Pt sites in our system. As illustrated in Figure S21, the binding of H atoms to Pt sites is relatively less stable than that to N most likely due to the presence of –OH groups nearby the Pt sites and the adsorption of CO_2 molecules at the Pt sites. As a result, the H atoms were more preferentially combined with C–N rings, which suppressed the H_2 evolution and provided H source for C–H bond formation. To support this argument, we calcinated Pt@Def-CN in a relatively mild environment (250 °C) to control the structural defects. With the extension of calcination time, the structural defects slowly diminished without the aggregation of single Pt atoms, and as a result, the surface –OH groups were greatly reduced (Figure S22). It turned out that without –OH groups, the yield of CH_4 decreased significantly and the main product became H_2 (Figure S23). Based on the examination of samples with different defect concentrations, we can safely draw the conclusion that the defects with –OH groups contribute to the improvement of product selectivity toward CO_2 methanation.

Conclusion

In summary, a catalyst for photocatalytic CO_2 methanation with H_2O was successfully designed at the atomic scale by introducing single Pt atoms to defect locations of CN along with creation of –OH groups. This photocatalyst exhibited high photocatalytic CO_2 reduction activity (6.3 $\mu mol\, g^{-1} h^{-1}$ CH_4 evolution) and CH_4 selectivity (99 %) in a pure water system. Thanks to the –OH groups, a large amount of CO_2 was enriched over the catalyst surface. Subsequently, single Pt atoms can localize the photogenerated electrons to activate the adsorbed CO_2 and to form CH_4 by subsequent hydrogenation. In the meantime, the photogenerated holes, left on the CN, reacted with H_2O to produce *H and O_2 to provide hydrogen source. During this process, single Pt atoms effectively reduced the energy barrier of the rate-limiting step to accelerate the reaction as well as increase the *CO desorption energy to improve the selectivity of CH_4. Note that the Pt sites did not play a major role for H_2 evolution, given the unique environment created by –OH groups and adsorbed CO_2. Taken together, our experimental characterization and theoretical calculation have demonstrated the mechanism that single Pt sites, CN defects and –OH groups synergistically work for different functions. This finding provides a new insight for the design of photocatalysts at the atomic scale to trigger enhanced CO_2 photoreduction into CH_4.

Acknowledgements

This work was supported by the National Key Research and Development Program of China (grant No. 2016YFA0203000), National Natural Science Foundation of China (grant Nos. 51878644, 21725102 and 41573138), and Strategic Priority Research Program of the Chinese Academy of Sciences (grant Nos. XDA23010300 and XDA23010000).

Conflict of Interest

The authors declare no conflict of interest.

Data Availability Statement

The data that support the findings of this study are available from the corresponding author upon reasonable request.

Keywords: Active Sites · CO_2 Methanation · Defect Engineering · Polymeric Carbon Nitride · Single-Atom Catalysts

[1] a) C. S. Diercks, Y. Liu, K. E. Cordova, O. M. Yaghi, *Nat. Mater.* **2018**, *17*, 301–307; b) J. L. White, M. F. Baruch, J. E. Pander III, Y. Hu, I. C. Fortmeyer, J. E. Park, T. Zhang, K. Liao, J. Gu, Y. Yan, T. W. Shaw, E. Abelev, A. B. Bocarsly, *Chem. Rev.* **2015**, *115*, 12888–12935; c) H. Rao, L. C. Schmidt, J. Bonin, M. Robert, *Nature* **2017**, *548*, 74–77; d) W. Gao, S. Li, H. He, X. Li, Z. Cheng, Y. Yang, J. Wang, Q. Shen, X. Wang, Y. Xiong, Y. Zhou, Z. Zou, *Nat. Commun.* **2021**, *12*, 4747.

[2] S. N. Habisreutinger, L. Schmidt-Mende, J. K. Stolarczyk, *Angew. Chem. Int. Ed.* **2013**, *52*, 7372–7408; *Angew. Chem.* **2013**, *125*, 7516–7557.

[3] X. Jiao, X. Li, X. Jin, Y. Sun, J. Xu, L. Liang, H. Ju, J. Zhu, Y. Pan, W. Yan, Y. Lin, Y. Xie, *J. Am. Chem. Soc.* **2017**, *139*, 18044–18051.

[4] T. Zhang, W. Lin, *Chem. Soc. Rev.* **2014**, *43*, 5982–5993.

[5] C. Gao, S. Chen, Y. Wang, J. Wang, X. Zheng, J. Zhu, L. Song, W. Zhang, Y. Xiong, *Adv. Mater.* **2018**, *30*, 1704624.
[6] W. J. Ong, L. L. Tan, Y. H. Ng, S. T. Yong, S. P. Chai, *Chem. Rev.* **2016**, *116*, 7159–7329.
[7] a) Z. Jiang, X. Xu, Y. Ma, H. S. Cho, D. Ding, C. Wang, J. Wu, P. Oleynikov, M. Jia, J. Cheng, Y. Zhou, O. Terasaki, T. Peng, L. Zan, H. Deng, *Nature* **2020**, *586*, 549–554; b) E. M. Nichols, J. J. Gallagher, C. Liu, Y. Su, J. Resasco, Y. Yu, Y. Sun, P. Yang, M. C. Y. Chang, C. J. Chang, *Proc. Natl. Acad. Sci. USA* **2015**, *112*, 11461–11466; c) X. Zhang, X. Li, D. Zhang, N. Q. Su, W. Yang, H. O. Everitt, J. Liu, *Nat. Commun.* **2017**, *8*, 14542; d) S. F. Ji, Y. Qu, T. Wang, Y. N. Chen, G. F. Wang, X. Li, J. C. Dong, Q. Y. Chen, W. Y. Zhang, Z. D. Zhang, S. Y. Liang, R. Yu, Y. Wang, D. S. Wang, Y. D. Li, *Angew. Chem. Int. Ed.* **2020**, *59*, 10651–10657; *Angew. Chem.* **2020**, *132*, 10738–10744.
[8] a) O. K. Varghese, M. Paulose, T. J. LaTempa, C. A. Grimes, *Nano Lett.* **2009**, *9*, 731–737; b) Y. Cao, L. Guo, M. Dan, D. E. Doronkin, C. Han, Z. Rao, Y. Liu, J. Meng, Z. Huang, K. Zheng, P. Chen, F. Dong, Y. Zhou, *Nat. Commun.* **2021**, *12*, 1675.
[9] L. M. Wang, W. L. Chen, D. D. Zhang, Y. P. Du, R. Amal, S. Z. Qiao, J. W. Bf, Z. Y. Yin, *Chem. Soc. Rev.* **2019**, *48*, 5310–5349.
[10] J. Fu, K. Liu, K. Jiang, H. Li, P. An, W. Li, N. Zhang, H. Li, X. Xu, H. Zhou, D. Tang, X. Wang, X. Qiu, M. Liu, *Adv. Sci.* **2019**, *6*, 1900796.
[11] L. Jiang, X. Yuan, Y. Pan, J. Liang, G. Zeng, Z. Wu, H. Wang, *Appl. Catal. B* **2017**, *217*, 388–406.
[12] J. Fu, J. Yu, C. Jiang, B. Cheng, *Adv. Energy Mater.* **2018**, *8*, 1701503.
[13] T. W. van Deelen, C. H. Mejia, K. P. de Jong, *Nat. Catal.* **2019**, *2*, 955–970.
[14] a) Y. Ren, Y. Tang, L. Zhang, X. Liu, L. Li, S. Miao, D. Sheng Su, A. Wang, J. Li, T. Zhang, *Nat. Commun.* **2019**, *10*, 4500; b) Y. Chen, S. Ji, W. Sun, Y. Lei, Q. Wang, A. Li, W. Chen, G. Zhou, Z. Zhang, Y. Wang, L. Zheng, Q. Zhang, L. Gu, X. Han, D. Wang, Y. Li, *Angew. Chem. Int. Ed.* **2020**, *59*, 1295–1301; *Angew. Chem.* **2020**, *132*, 1311–1317; c) R. Arrigo, M. E. Schuster, Z. Xie, Y. Yi, G. Wowsnick, L. L. Sun, K. E. Hermann, M. Friedrich, P. Kast, M. Hävecker, A. Knop-Gericke, R. Schlögl, *ACS Catal.* **2015**, *5*, 2740–2753.
[15] a) C. Chu, Q. Zhu, Z. Pan, S. Gupta, D. Huang, Y. Du, S. Weon, Y. Wu, C. Muhich, E. Stavitski, K. Domen, J. H. Kim, *Proc. Natl. Acad. Sci. USA* **2020**, *117*, 6376–6382; b) E. Vorobyeva, E. Fako, Z. Chen, S. M. Collins, D. Johnstone, P. A. Midgley, R. Hauert, O. V. Safonova, G. Vile, N. Lopez, S. Mitchell, J. Perez-Ramirez, *Angew. Chem. Int. Ed.* **2019**, *58*, 8724–8729; *Angew. Chem.* **2019**, *131*, 8816–8821; c) W. Liu, L. L. Cao, W. R. Cheng, Y. J. Cao, X. K. Liu, W. Zhang, X. L. Mou, L. L. Jin, X. S. Zheng, W. Che, Q. H. Liu, T. Yao, S. Q. Wei, *Angew. Chem. Int. Ed.* **2017**, *56*, 9312–9317; *Angew. Chem.* **2017**, *129*, 9440–9445.
[16] X. G. Li, W. T. Bi, L. Zhang, S. Tao, W. S. Chu, Q. Zhang, Y. Luo, C. Z. Wu, Y. Xie, *Adv. Mater.* **2016**, *28*, 2427–2431.
[17] L. Zhang, R. Long, Y. Zhang, D. Duan, Y. Xiong, Y. Zhang, Y. Bi, *Angew. Chem. Int. Ed.* **2020**, *59*, 6224–6229; *Angew. Chem.* **2020**, *132*, 6283–6288.
[18] A. Thomas, A. Fischer, F. Goettmann, M. Antonietti, J.-O. Mueller, R. Schloegl, J. M. Carlsson, *J. Mater. Chem.* **2008**, *18*, 4893–4908.
[19] W. Jiang, Q. Ruan, J. Xie, X. Chen, Y. Zhu, J. Tang, *Appl. Catal. B* **2018**, *236*, 428–435.
[20] Z. Zeng, Y. Su, X. Quan, W. Choi, G. Zhang, N. Liu, B. Kim, S. Chen, H. Yu, S. Zhang, *Nano Energy* **2020**, *69*, 104409.
[21] Y. R. Li, Z. W. Wang, T. Xia, H. X. Ju, K. Zhang, R. Long, Q. Xu, C. M. Wang, L. Song, J. F. Zhu, J. Jiang, Y. J. Xiong, *Adv. Mater.* **2016**, *28*, 6959–6965.
[22] Y. Wang, Z. Zhang, L. Zhang, Z. Luo, J. Shen, H. Lin, J. Long, J. C. S. Wu, X. Fu, X. Wang, C. Li, *J. Am. Chem. Soc.* **2018**, *140*, 14595–14598.
[23] J. Di, C. Chen, S. Yang, S. Chen, M. Duan, J. Xiong, C. Zhu, R. Long, W. Hao, Z. Chi, H. Chen, Y.-X. Weng, J. Xia, L. Song, S. Li, H. Li, Z. Liu, *Nat. Commun.* **2019**, *10*, 2840.
[24] S. Wang, Y. Gao, S. Miao, T. Liu, L. Mu, R. Li, F. Fan, C. Li, *J. Am. Chem. Soc.* **2017**, *139*, 11771–11778.
[25] C. Kai, X. Sun, Y. Jia, Z. Shi, K. Jiang, J. Ben, Y. Wu, Y. Wang, H. Liu, X. Li, D. Li, *Sci. China-Phys. Mech. Astron.* **2019**, *62*, 067311.
[26] L. Bi, X. Gao, L. Zhang, D. Wang, X. Zou, T. Xie, *ChemSusChem* **2018**, *11*, 276–284.
[27] a) M. Kong, Y. Z. Li, X. Chen, T. T. Tian, P. F. Fang, F. Zheng, X. J. Zhao, *J. Am. Chem. Soc.* **2011**, *133*, 16414–16417; b) Y. C. Zhang, N. Afzal, L. Pan, X. W. Zhang, J. J. Zou, *Adv. Sci.* **2019**, *6*, 1900053.
[28] M. J. Liu, P. F. Xia, L. Y. Zhang, B. Cheng, J. G. Yu, *ACS Sustainable Chem. Eng.* **2018**, *6*, 10472–10480.
[29] A. Li, Q. Cao, G. Zhou, B. Schmidt, W. Zhu, X. Yuan, H. Huo, J. Gong, M. Antonietti, *Angew. Chem. Int. Ed.* **2019**, *58*, 14549–14555; *Angew. Chem.* **2019**, *131*, 14691–14697.
[30] a) Y. L. Yang, F. Li, J. Chen, J. J. Fan, Q. J. Xiang, *ChemSusChem* **2020**, *13*, 1979–1985; b) Y. Wang, J. Zhao, T. Wang, Y. Li, X. Li, J. Yin, C. Wang, *J. Catal.* **2016**, *337*, 293–302; c) Z. Sun, J. M. T. A. Fischer, Q. Li, J. Hu, Q. Tang, H. Wang, Z. Wu, M. Hankel, D. J. Searles, L. Wang, *Appl. Catal. B* **2017**, *216*, 146–155.
[31] a) L. C. Grabow, M. Mavrikakis, *ACS Catal.* **2011**, *1*, 365–384; b) H. D. She, Y. Wang, H. Zhou, Y. Li, L. Wang, J. W. Huang, Q. Z. Wang, *ChemCatChem* **2019**, *11*, 753–759.
[32] P. Xia, B. Zhu, J. Yu, S. Cao, M. Jaroniec, *J. Mater. Chem. A* **2017**, *5*, 3230–3238.
[33] G. P. Gao, Y. Jiao, E. R. Waclawik, A. J. Du, *J. Am. Chem. Soc.* **2016**, *138*, 6292–6297.
[34] C. Dong, C. Lian, S. Hu, Z. Deng, J. Gong, M. Li, H. Liu, M. Xing, J. Zhang, *Nat. Commun.* **2018**, *9*, 1252.

Manuscript received: February 25, 2022
Accepted manuscript online: April 27, 2022
Version of record online: May 6, 2022